






Precise study of triply charmed baryons (Ω_{ccc})

Navdeep Singh Dhindsa ^{1,*} Debsubhra Chakraborty ^{2,†} Archana Radhakrishnan ^{2,‡} Nilmani Mathur ^{2,§} and M. Padmanath ^{1,3,¶}

¹*The Institute of Mathematical Sciences, CIT Campus, Chennai, 600113, India*

²*Department of Theoretical Physics, Tata Institute of Fundamental Research, Homi Bhabha Road, Mumbai 400005, India*

³*Homi Bhabha National Institute, Training School Complex, Anushaktinagar, Mumbai 400094, India*

We present the most precise results for the ground state mass of the triply-charmed spin-3/2 baryon using lattice quantum chromodynamics. The calculations are performed on six $N_f = 2 + 1 + 1$ Highly Improved Staggered Quark (HISQ) lattice ensembles generated by the MILC collaboration. Two different lattice setups are employed: in the first one, a fully dynamical calculation with HISQ action is performed, while in the second calculation, an overlap action is utilized for the valence charm quark dynamics. Following the continuum extrapolation of our results, obtained at five different lattice spacings, two different volumes, and two different actions, our prediction for the mass of the lowest triply charmed spin-3/2 baryon, $\Omega_{ccc}(3/2^+)$, is 4793(5)(7) MeV. This is the most precise determination to date, fully addressing the systematic uncertainties. We also predict the $\Omega_{ccc}(3/2^-)$ mass to be 5094(12)(13) MeV.

The role of single-flavored baryons was paramount in identifying the color degrees of freedom and the subsequent development of quantum chromodynamics (QCD), the theory of strong interactions. The discovery of $\Omega(sss)(J^P = 3/2^+)$ baryon firmly established the quark model as an effective phenomenological framework for describing subatomic particles, which further lead to many key advancements in our understanding of nuclear and particle physics. Although the single-flavored baryons have only been discovered with light and strange flavors (Δ and Ω), the existence of their counterparts with charm and bottom flavors—namely Ω_{ccc} and Ω_{bbb} —is beyond any doubt within QCD. The Ω_{QQQ} ($Q \equiv c, b$) baryons, which are baryon analogues of heavy quarkonia, offer a simplistic system for studying quark-quark interactions and quark confinement without the complexities of valence light quark dynamics [1–3]. As pointed out by Bjorken, such baryons may provide a new window for understanding the internal parton level dynamics within baryons [1]. These baryons are expected to be discovered as experimental facilities reach the required center-of-momentum energy and luminosity, with Ω_{ccc}^{++} likely being the first to be observed. Precise theoretical predictions using first principles calculations of QCD can guide the experiments in discovering the $\Omega_{ccc}^{++}(3/2^+)$ baryon. In this work, we present the most precise determination of the ground state mass of the $\Omega_{ccc}^{++}(3/2^+)$ baryon using the first-principles lattice QCD methodology, carefully accounting both statistical and all potential systematic uncertainties, which ensures that the final mass prediction is reliable and accurate.

Since the strong decay of the lightest spin-3/2 Ω_{ccc} baryon is forbidden, it should have a relatively long

lifetime. Probable decay modes, where they could be searched for, are semileptonic decay processes such as $\Omega_{ccc}^{++} \rightarrow \Omega_{ccs}^+ + \{l\} \rightarrow \Xi_{ccu}^{++} + 2\{l\}$, $\Omega_{ccc}^{++} \rightarrow \Xi_{ccd}^+ + \{l\}$, among others ($\{l\}$ refers to lepton pair involved in the decay). Direct detection of such long lived particles could be difficult, unless the lighter hadrons to which they decay are well understood. However, recent experimental reports on tri- J/ψ production [4], and recent proposals of inclusive search strategies [5, 6] and extensions of new sensitive timing based variables [7] to identify signatures for long lived hadrons augment promising prospects for the discovery of Ω_{ccc}^{++} baryons in the near future.

Considering the heavy quark constituents within, it is expected that the phenomenological models would be able to reliably predict the masses of Ω_{ccc} baryons. Indeed, within model calculations, starting with early works of Bjorken [1], these baryons have been studied with non-relativistic [8–14] and relativistic [15, 16] quark models, QCD sum rule [17–21], Faddeev equation [22–24], di-quark model [25, 26], variational method [27, 28], bag model [29, 30], hypercentral constituent quark model [31–33], Regge theory [34], Bethe-Salpeter equation [35] and renormalization group procedure for effective particles approach [36]. However, depending on the model parameters, these predictions are spread over 400 MeV uncertainty.

In this context, first principles lattice QCD calculations with controlled systematics can play a vital role in narrowing the possible mass window for these baryons. Most importantly, lattice QCD calculations can rigorously incorporate non-perturbative aspects that may be overlooked by potential models and other phenomenological approaches. Several lattice QCD studies of Ω_{ccc} baryons have also already been performed, starting with studies using pure $SU(3)$ gauge theory [37], dynamical simulations with quenched charm quarks [2, 38–45], and those involving dynamical quarks up to charm flavor [46–50]. Most of these calculations were performed at a single lattice spacing, whereas addressing lattice artifacts through continuum extrapolation with several lattice

* navdeep.s.dhindsa@gmail.com

† debsubhra.chakraborty@tifr.res.in

‡ archana.radhakrishnan@tifr.res.in

§ nilmani@theory.tifr.res.in

¶ padmanath@imsc.res.in

spacings is essential to assess the systematic uncertainties from cutoff effects, particularly considering the presence of three heavy quarks in these baryons. The studies in Refs. [38, 40, 46, 47, 50] have performed continuum extrapolation with up to three lattice spacings, leading to mass estimates for $\Omega_{ccc}(3/2^+)$ that are spread over a range of 100 MeV. There are no continuum extrapolated results for the mass of $3/2^-$ ground state, with existing predictions scattered over a 250 MeV energy interval.

It is therefore important to perform a systematic lattice QCD determination of the masses of low lying Ω_{ccc}^{++} baryons, with an accuracy similar to the state-of-the-art lattice determination of other hadrons, such as that in low-lying charmonia and proton. In this work, we present such a study utilizing up to six lattice QCD ensembles, five different lattice spacings, two lattice volumes and $N_f = 2 + 1 + 1$ Highly Improved Staggered Quark (HISQ) dynamics [51], generated by the MILC Collaboration [52, 53] (see Fig. 1, and Table I in Ref. [54]). In the valence sector, we employ two different approaches. In the first, a fully dynamical evaluation of the Ω_{ccc}^{++} baryon masses is made with HISQ action for the valence charm quark evolution. In the second approach, an overlap action [55, 56], which has no $\mathcal{O}(ma)$ error, is employed for the valence charm quark dynamics, similar to many of our previous publications [57–61]. With such a diverse and state-of-the-art setup of multiple lattice spacings, lattice volumes, and two different valence charm quark actions, we predict the ground state mass of $\Omega_{ccc}^{++}(3/2^+)$ baryon to be 4793(5)(7) MeV. The mass for the lowest $J^P \equiv 3/2^-$ state is also predicted with per mille precision. Below, we detail the methods and procedures employed to obtain these results.

We evaluate the hadron masses from the two point correlation functions with a wall source and a point sink smearing, where the correlators are fitted with an exponential form at large source-sink separation. Such a setup was demonstrated to be robust and reliable for extracting single-hadron masses, particularly for ground state heavy hadrons [60–62]. We also observe that to be the case for the Ω_{ccc} baryon masses studied in this work. The charm quark mass, being heavy, leads to relatively clean and stable signals. Further, to mitigate the excited state effects from the extracted ground state hadron masses, we evaluate correlation matrices that are analyzed variationally following the solutions of a generalized eigenvalue problem [63, 64]. Further details can be found in Sections II and III of Ref. [54].

Ω_{ccc} baryons with valence overlap fermions:– In this setup, we utilize only spatially local interpolators, (\mathcal{O}_b). This is well justified considering the predicted smaller charge radius of Ω_{ccc} [41]. The trivial flavor symmetry and color antisymmetry imply the total spin structure for the Ω_{ccc} baryon interpolator has to be symmetric. With a four component fermion spinor in the Dirac-Pauli representation of Dirac- γ matrices [65] with $\gamma_4 = \text{diag}[1, 1, -1, -1]$ representing the quark fields, one can have two embeddings of finite volume irrep H ($\in \{\Lambda_{O_h}\}$) possessing fully

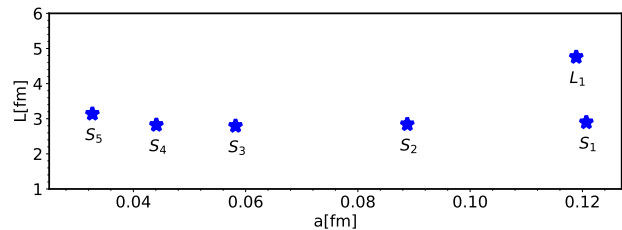


FIG. 1. Six lattice QCD ensembles used in this work and are labeled in the plot as S₅ ($96^3 \times 288$), S₄ ($64^3 \times 192$), S₃ ($48^3 \times 144$), S₂ ($32^3 \times 96$), S₁ ($24^3 \times 64$), and L₁ ($40^3 \times 64$).

symmetric spin structure and with spin-3/2 being the lowest contributing spin [2, 66]. Here, Λ_{O_h} refers to the irrep of the Octahedral group O_h . Correlation matrices are evaluated using the operator basis composed of these two operators and are then analyzed following variational techniques [63, 64]. The symmetry properties of baryon correlators under fermionic temporal boundary conditions provide additional advantage in improvising the signal for baryon mass estimates [67–69]. Further details on this are provided in Section II of the supplement [54].

Ω_{ccc} baryons with HISQ fermions:– The $\Omega_{sss}(3/2^+)$ has been studied with HISQ valence quark previously [70], and following that we use the following interpolating field for $\Omega_{ccc}(3/2^+)$,

$$\mathcal{O}_{\Omega_{ccc}}(t) = \epsilon_{abc} D_1 c^a(\mathbf{x}, t) D_2 c^b(\mathbf{x}, t) D_3 c^c(\mathbf{x}, t), \quad (1)$$

where $c^a(\mathbf{x}, t)$ is the HISQ charm quark field with (a, b, c) as the color indices, and D_i s are the spatial derivative operators [71]. Other details about this operator are given in the supplement [54]. Note that the operator in Eq.(1) couples with multiple tastes. However, the splittings between finite-volume ground state energy of Ω baryon of different tastes are expected to be small as HISQ action removes all taste-exchange effectively through one-loop order [51], and this has been shown in Ref. [70]. To reduce the effects of oscillating components of staggered correlators, the two-point correlators are first smoothed and the procedure is detailed in the supplement [54]. To determine the ground state masses, we employ two methods. The first one involves the standard large-time fit with a single exponential. We also use two-exponentials particularly for the spin-3/2⁻ state where the contamination from the excited states may not be insignificant. In the second method, we utilize the generalized eigenvalue problem (GEVP)[63, 64], using a matrix constructed from time-shifted correlation functions, as described in Ref. [72], allowing a robust estimation of the ground state.

Mass extraction and results:– In Fig. 2, we present two representative effective mass plots ($m_{eff} = \log[C(\tau + 1)/C(\tau)]$, $C(\tau)$ being the correlation function) for the lowest energy level of the $\Omega_{ccc}(3/2^+)$ state on ensembles with the finest two lattice spacings. The top pane corresponds to the case of valence overlap action on the $64^3 \times 192$ lattice, and the bottom pane is that with HISQ valence action on the $96^3 \times 288$ lattice. The horizontal bands

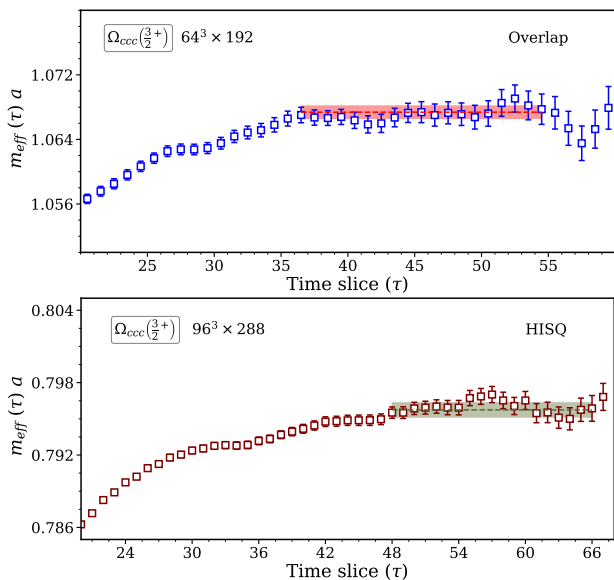


FIG. 2. Representative effective mass plots for the lowest energy state of $\Omega_{cc}(3/2^+)$ baryon. Top: overlap action, lattice size: $64^3 \times 192$, Bottom: HISQ action, lattice size $96^3 \times 288$.

represent the fit estimate with 1σ error. Further details of mass fits and results for other lattices and other hadrons studied are shown in the supplemental material [54].

The large bare quark mass ($m_Q a$) introduces significant discretization effects, which can be a primary source of systematic uncertainties in heavy hadrons, especially in those containing multiple heavy quarks. The leading discretization errors in the valence quark actions that we employ (overlap and HISQ) are at $\mathcal{O}((ma)^2)$. To further mitigate these errors, instead of estimating the masses directly, we follow the practice of studying mass splittings, where the valence heavy quark content is subtracted out as in Refs. [57–62]. Here we subtract out the valence charm quark content with the following choice,

$$a\Delta M_{\Omega_{ccc}} = [aM_{\Omega_{ccc}}^L - \frac{3}{2}aM_{c\bar{c}}^L], \quad (2)$$

where $aM_{\Omega_{ccc}}^L$ and $aM_{c\bar{c}}^L$ are the finite lattice estimates for the mass of Ω_{ccc} baryon and the reference charmonia energy ($c\bar{c}$), respectively. Two different choices for $c\bar{c}$ are considered in our analysis: J/ψ and the spin averaged $\overline{1S}$ state, $\frac{1}{4}(\eta_c + 3J/\psi)$. These choices are made considering that we tune the charm quark mass using $\overline{1S}$, while J/ψ masses on the lattice are found to be closer to its physical mass on each lattice. We perform the continuum extrapolation on these mass splittings, owing to the expectations of reduced cutoff effects on them. Here we prefer the reference energy with respect to the J/ψ meson mass as the estimation of the J/ψ mass on lattice is more accurate compared to the spin-averaged $\overline{1S}$ energy, potentially related to the dominant charm self-annihilation effects expected and also observed in η_c meson mass [73].

In Fig. 3 we show the continuum extrapolation of the mass splittings $\Delta M_{\Omega_{ccc}(3/2^+)}$ in physical units, with

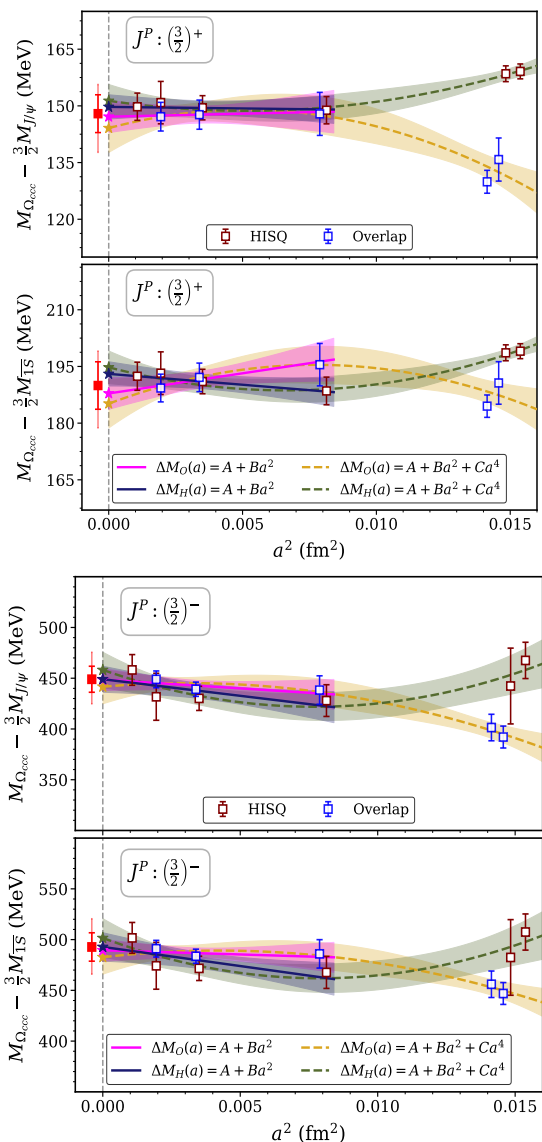


FIG. 3. Continuum extrapolations of the subtracted ground state masses $\Delta M_{\Omega_{ccc}}^{\text{sub}}(a)$ (Eq. 2). Top two: $\Omega_{ccc}(3/2^+)$ and bottom two: $\Omega_{ccc}(3/2^-)$. Subtraction of charm quark content is done with both $c\bar{c} \equiv J/\psi$ and $\overline{1S}$. Various fit forms with their respective color schemes are shown in the legends and more details on fits are provided in the supplement [54]. The shaded bands represent 1σ uncertainties, estimated via the bootstrap method. Symbol star: continuum extrapolated values. Red solid square: final value by symmetrized averaging the linear fit results of overlap and HISQ quarks, while the extended errors include other fits results.

the top two panes using $c\bar{c} \equiv J/\psi$ (top figure) and $c\bar{c} \equiv \overline{1S}$ (second from the top). We consider two possible cutoff dependence: (i) $\Delta M(a) = c_1 + c_2 a^2$, (ii) $\Delta M(a) = c_1 + c_2 a^2 + c_3 a^4$. Additionally, we use (iiia) a fitting form similar to Eq.(5) of Ref. [74] and (iiib) $\Delta M(a) = c_1 + c_2 a^2 + c_3 \alpha_s(1/a)(m_c a)^2$ for the HISQ results. The marker and coloring convention used are explained in the figure and its caption. The bottom two

figures, with the same color-coding and fit forms, represent the continuum extrapolation for the $\Omega_{ccc}(3/2^-)$ baryon. Once the continuum extrapolated value of $\Delta M_{\Omega_{ccc}}^{cont}$ is obtained, we add that to the physical value of $\frac{3}{2}M_{c\bar{c}}^{exp}$ to obtain the physical estimates for baryon mass, as in,

$$M_{\Omega_{ccc}}^{phys} = [\Delta M_{\Omega_{ccc}}^{cont} + \frac{3}{2}M_{c\bar{c}}^{exp}]. \quad (3)$$

A clear agreement can be observed between the $\Omega_{ccc}(3/2^+)$ estimates using the overlap as well as the HISQ action across finer lattices leading to a consistent continuum extrapolated value. Our final result, represented by the red square at the continuum point, is a symmetrized average of the HISQ (green star) and overlap (blue star) results obtained from linear fits to the finest lattice points (starting at $a = 0.0888$ fm), with the magenta and blue bands representing the fitted results for the HISQ and overlap actions, respectively. The associated fit error, indicated by the thick red line, encompasses the fit errors for both the overlap and HISQ actions and is quoted as the statistical error. The thin red line illustrates the range of fit errors (bootstrap) arising from variations in lattice spacing dependence and differences in actions (as shown in Table III of the supplement [54]). The deviations of the thin red line from the thick red line are included in our systematic errors. As previously discussed, using $c\bar{c} \equiv J/\psi$ provides a more reliable basis for continuum extrapolation, and our final values are quoted accordingly. Our final estimates are $M_{\Omega_{ccc}}(3/2^+) = 4793(5)(7)$ MeV, and $M_{\Omega_{ccc}}(3/2^-) = 5094(12)(13)$ MeV, where the first error is statistical and the second one accounts for all other possible systematic errors, which we will discuss next. We also estimate the mass splitting between these two baryons to be: $\Delta_{\Omega_{ccc}}(3/2^+ - 3/2^-) = 301(13)(14)$ MeV. Note that for reliable estimation of $\Omega_{ccc}(3/2^-)$ mass, one needs to consider the presence of a nearby three hadron final state $\Omega_{ccc}(3/2^+)\pi\pi$ in P -wave in the chiral limit. However, investigating such contamination is beyond the scope of this work. If the three quark Fock component of the negative parity state were dominant and its coupling with the three hadron state be negligible, we anticipate our estimate would be reliable.

Error estimation – Below, we address the estimation of various errors related to this work.

Statistical– In this, we include bootstrap fit error, including various possible choices of fit-windows, and the final value includes the fit-error covering both overlap and HISQ results.

Discretization– Here, we include the difference in fit values obtained using different fit forms with two different discretized lattice actions.

Scale setting– Measurements of scale with Wilson flow and r_1 parameter are found to be consistent for these lattice ensembles. Including the scale setting errors we find the uncertainty in mass difference (Eq. 2) for Ω to be ~ 3 MeV.

Charm quark mass tuning: After tuning the charm quark mass on each lattice (as detailed in the supplement [54]),

we calculate the mass splittings (Eq. (2), at its central value and at its variations. The effect on mass splittings was found to be, at most, 2 MeV.

Taste splitting (HISQ)– For HISQ valence quarks this effect leads to a difference in masses at finite lattice spacing with a $\mathcal{O}(\alpha_s(1/a)(m_c a)^2)$ mixing between two tastes of Ω_{ccc} baryons. We account for that in the continuum extrapolation, which leads to an error of 2 MeV.

Mixed action effect (Overlap)– In the overlap setup, unitarity violations arise for two reasons [75–77]. One is related to the difference in action used in the sea and valence sectors, which is expected to die out in the continuum limit [78]. In the same lattice setup (with $a = 0.0582$ fm), we found this effect to be small [78]. The second one is related to the sea and valence charm quark mass difference, which could survive in the continuum [77]. The difference in estimates from the HISQ valence action and the overlap valence action already reflects these systematics. Based on the disagreement between the numbers from these two scenarios in the common finest lattice, we assign a conservative estimate of 2 MeV to account for this systematic.

Finite volume– A lattice QCD study [41] on electromagnetic properties inferred that the $\Omega_{ccc}^{++}(3/2^+)$ has a small charge radius, $r_c = 0.410(6)$ fm, which is smaller than the typical size of a baryon. The two lattice volumes that we use for this work have sizes of about 3 and 4.8 fm which are much bigger than the above-mentioned charge-diameter. Result extracted in two different volumes are also consistent with each other.

Electromagnetism– The presence of two units of charge is expected to influence the mass of a Ω_{ccc}^{++} baryon. A perturbative estimate, as shown in the supplement [54], yields a correction term < 5 MeV. In Ref. [44] the Coulomb repulsion in a dibaryon, made with six charm quarks and having four units of charge, was found to be about 5 MeV. Given the constituent composition of Ω_{ccc}^{++} relative to that system, we anticipate that the mass correction from Coulomb effects could be comparatively smaller. Additionally, the magnetic moment of Ω_{ccc}^{++} has been predicted to be about $1 \mu_N$ [79] suggesting no large effect on its mass. Based on these factors we assign an uncertainty of 4 MeV to its mass. However, a direct calculation would be necessary for a more rigorous assessment of these effects, but that lies beyond the scope of the present work.

Other errors– There is no systematic due to chiral extrapolation. For these all-heavy baryons with no valence light quark content, the effect of unphysical sea quark masses is expected to be minimal [80–82] and should be absorbed within the statistical error.

Based on the above estimation, we summarize the error budget in Table I below.

In Fig. 4, we summarize the results on the ground state mass of $\Omega_{ccc}(3/2)$ baryons showing our results (red circles at the bottom / vertical blue band) and compare it with previous results. The vertical blue band serves as a reference point for comparing other findings with our results. A horizontal dashed line is placed to separate

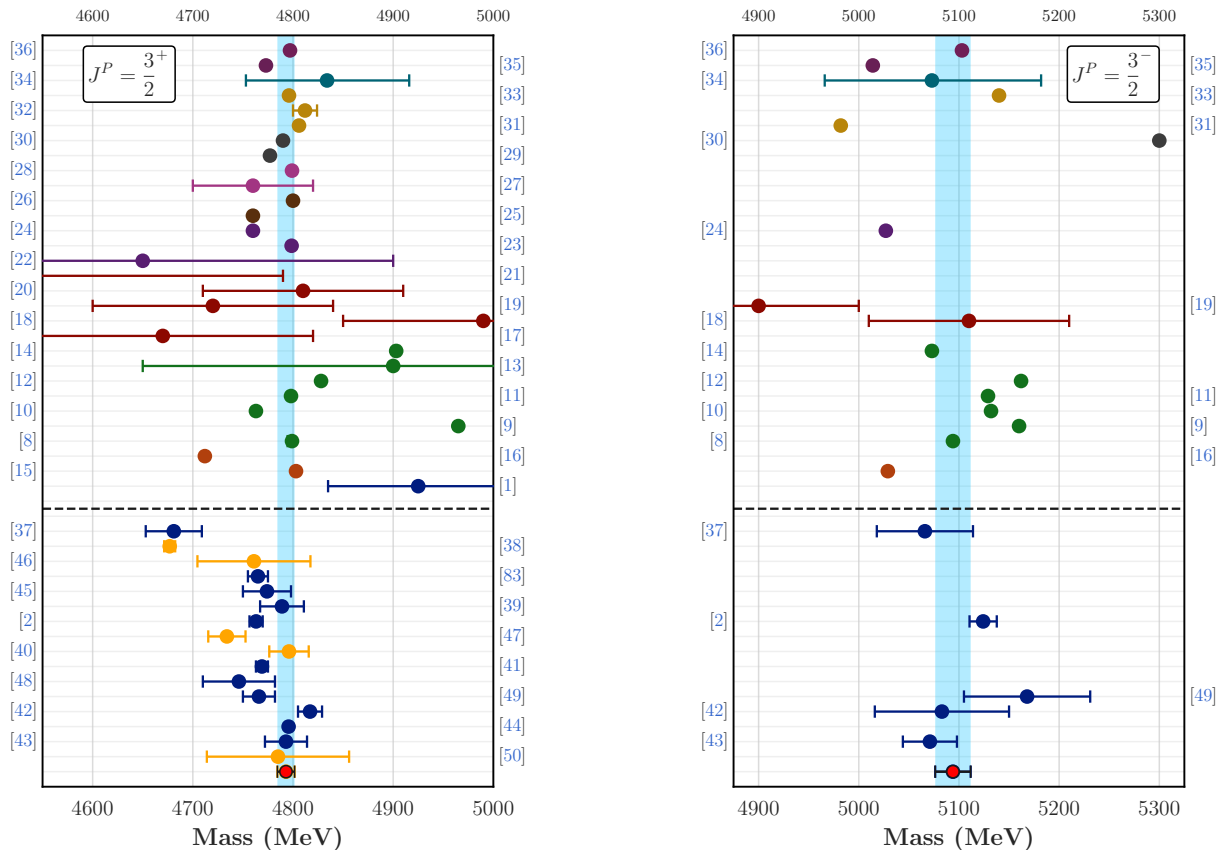


FIG. 4. Summary of results on the ground state mass of $\Omega_{ccc}(3/2^+)$ (left) and $\Omega_{ccc}(3/2^-)$ (right) baryons as obtained in various calculations (references on the side panels can be tracked through the faint horizontal lines). The results below the thick horizontal dashed line are from lattice calculations and above that are obtained using various models. Among the lattice results, those with orange circles are obtained with continuum extrapolations, while others (blue circles) are obtained at a single lattice spacing. Our results at the physical point are shown by the red circles (at the bottom)

Source	Error (MeV)
Statistical	5
Discretization	4
Scale setting	3
m_c tuning	2
Taste-splitting (HISQ)	2
Mixed action (Overlap)	2
Finite size	1
Electromagnetism	4
Total	5 (stat) & 7 (syst)

TABLE I. Error budget in the calculation of the ground state mass of $\Omega_{ccc}^{++}(3/2^+)$ baryon.

lattice and non-lattice results (see caption). Lattice results are also color-coded to distinguish those that include continuum extrapolation from those that do not (*c.f.* see Table X in supplement [54] for more details). It is evident this work clearly narrows down the broad range of estimates from previous calculations, providing the most precise lattice results to date while properly addressing

the associated systematic uncertainties. It is also worth noting that some model results align closely with the vertical line, suggesting it may be interesting to explore possible commonalities in their interaction potentials that lead to results near our lattice estimation.

NSD, DC, and AR have contributed equally and are credited as co-first authors.

This work is supported by the Department of Atomic Energy, Government of India, under Project Identification Number RTI 4002. Computations were carried out on the Cray-XC30 of ILGTI, TIFR (which has recently been closed), and the computing clusters at the Department of Theoretical Physics, TIFR, Mumbai, and ISc Chennai. We are thankful to the MILC collaboration and, in particular, to S. Gottlieb for providing us with the HISQ lattice ensembles. We would also like to thank Ajay Salve, Kapil Ghadiali, and T. Chandramohan for computational support. NM and DC also thank Amol Dighe for discussions. MP gratefully acknowledges support from the Department of Science and Technology, India, SERB Start-up Research Grant No. SRG/2023/001235.

-
- [1] J. D. Bjorken, Is the ccc a new deal for baryon spectroscopy?, *AIP Conf. Proc.* **132**, 390 (1985).
- [2] M. Padmanath, R. G. Edwards, N. Mathur, and M. Pearson, Spectroscopy of triply-charmed baryons from lattice QCD, *Phys. Rev. D* **90**, 074504 (2014).
- [3] S. Meinel, Excited-state spectroscopy of triply-bottom baryons from lattice QCD, *Phys. Rev. D* **85**, 114510 (2012).
- [4] A. Tumasyan *et al.* (CMS), Observation of triple J/ψ meson production in proton-proton collisions, *Nature Phys.* **19**, 338 (2023), [Erratum: *Nature Phys.* **19**, (2023)].
- [5] T. Gershon and A. Poluektov, Displaced B_c^- mesons as an inclusive signature of weakly decaying double beauty hadrons, *JHEP* **01**, 019.
- [6] Q. Qin, Y.-J. Shi, W. Wang, G.-H. Yang, F.-S. Yu, and R. Zhu, Inclusive approach to hunt for the beauty-charmed baryons Ξ_{bc} , *Phys. Rev. D* **105**, L031902 (2022).
- [7] B. Bhattacharjee, T. Ghosh, R. Sengupta, and P. Solanki, Dedicated triggers for displaced jets using timing information from electromagnetic calorimeter at HL-LHC, *JHEP* **08**, 254.
- [8] B. Silvestre-Brac, Spectrum and static properties of heavy baryons, *Few Body Syst.* **20**, 1 (1996).
- [9] W. Roberts and M. Pervin, Heavy baryons in a quark model, *Int. J. Mod. Phys. A* **23**, 2817 (2008).
- [10] J. Vijande, A. Valcarce, and H. Garcilazo, Constituent-quark model description of triply heavy baryon nonperturbative lattice QCD data, *Phys. Rev. D* **91**, 054011 (2015).
- [11] G. Yang, J. Ping, P. G. Ortega, and J. Segovia, Triply heavy baryons in the constituent quark model, *Chin. Phys. C* **44**, 023102 (2020).
- [12] M.-S. Liu, Q.-F. Lü, and X.-H. Zhong, Triply charmed and bottom baryons in a constituent quark model, *Phys. Rev. D* **101**, 074031 (2020).
- [13] F. J. Llanes-Estrada, O. I. Pavlova, and R. Williams, A First Estimate of Triply Heavy Baryon Masses from the pNRQCD Perturbative Static Potential, *Eur. Phys. J. C* **72**, 2019 (2012).
- [14] E. Ortiz-Pacheco and R. Bijker, Masses and radiative decay widths of s - and p -wave singly, doubly, and triply heavy charm and bottom baryons, *Phys. Rev. D* **108**, 054014 (2023).
- [15] A. P. Martynenko, Ground-state triply and doubly heavy baryons in a relativistic three-quark model, *Phys. Lett. B* **663**, 317 (2008).
- [16] R. N. Faustov and V. O. Galkin, Triply heavy baryon spectroscopy in the relativistic quark model, *Phys. Rev. D* **105**, 014013 (2022).
- [17] J.-R. Zhang and M.-Q. Huang, Deciphering triply heavy baryons in terms of QCD sum rules, *Phys. Lett. B* **674**, 28 (2009).
- [18] Z.-G. Wang, Analysis of the triply-heavy baryon states with the QCD sum rules, *AAPPS Bull.* **31**, 5 (2021).
- [19] T. M. Aliev, K. Azizi, and M. Savcı, Properties of triply heavy spin-3/2 baryons, *J. Phys. G* **41**, 065003 (2014).
- [20] Z.-G. Wang, Analysis of the $\frac{3}{2}^+$ heavy and doubly heavy baryon states with QCD sum rules, *Eur. Phys. J. C* **68**, 459 (2010).
- [21] R.-H. Wu, Y.-S. Zuo, C. Meng, Y.-Q. Ma, and K.-T. Chao, NLO effects for Ω QQQ baryons in QCD Sum Rules, *Chin. Phys. C* **45**, 093103 (2021).
- [22] H. Sanchis-Alepuz, R. Alkofer, G. Eichmann, and R. Williams, Model Comparison of Delta and Omega Masses in a Covariant Faddeev Approach, *PoS QCD-TNT-II*, 041 (2011).
- [23] M. Radin, S. Babaghodrat, and M. Monemzadeh, Estimation of heavy baryon masses Ω_{ccc}^{++} and Ω_{bbb}^- by solving the faddeev equation in a three-dimensional approach, *Phys. Rev. D* **90**, 047701 (2014).
- [24] S.-x. Qin, C. D. Roberts, and S. M. Schmidt, Spectrum of light- and heavy-baryons, *Few Body Syst.* **60**, 26 (2019).
- [25] K. Thakkar, A. Majethiya, and P. C. Vinodkumar, Magnetic moments of baryons containing all heavy quarks in the quark-diquark model, *Eur. Phys. J. Plus* **131**, 339 (2016).
- [26] P.-L. Yin, C. Chen, G. a. Krein, C. D. Roberts, J. Segovia, and S.-S. Xu, Masses of ground-state mesons and baryons, including those with heavy quarks, *Phys. Rev. D* **100**, 034008 (2019).
- [27] Y. Jia, Variational study of weakly coupled triply heavy baryons, *JHEP* **10**, 073.
- [28] J. M. Flynn, E. Hernandez, and J. Nieves, Triply Heavy Baryons and Heavy Quark Spin Symmetry, *Phys. Rev. D* **85**, 014012 (2012).
- [29] A. Bernotas and V. Simonis, Heavy hadron spectroscopy and the bag model, *Lith. J. Phys.* **49**, 19 (2009).
- [30] P. Hasenfratz, R. R. Horgan, J. Kuti, and J. M. Richard, Heavy Baryon Spectroscopy in the QCD Bag Model, *Phys. Lett. B* **94**, 401 (1980).
- [31] Z. Shah and A. K. Rai, Masses and Regge trajectories of triply heavy Ω_{ccc} and Ω_{bbb} baryons, *Eur. Phys. J. A* **53**, 195 (2017).
- [32] B. Patel, A. Majethiya, and P. C. Vinodkumar, Masses and Magnetic moments of Triply Heavy Flavour Baryons in Hypercentral Model, *Pramana* **72**, 679 (2009).
- [33] N. Tazimi and A. Ghasempour, Mass spectrum of triply heavy baryon in the hypercentral quark model, *Modern Physics Letters A* **36**, 2150270 (2021).
- [34] K.-W. Wei, B. Chen, and X.-H. Guo, Masses of doubly and triply charmed baryons, *Phys. Rev. D* **92**, 076008 (2015).
- [35] S. Migura, D. Merten, B. Metsch, and H.-R. Petry, Charmed baryons in a relativistic quark model, *Eur. Phys. J. A* **28**, 41 (2006).
- [36] K. Serafin, M. Gómez-Rocha, J. More, and S. D. Glazek, Approximate Hamiltonian for baryons in heavy-flavor QCD, *Eur. Phys. J. C* **78**, 964 (2018).
- [37] T.-W. Chiu and T.-H. Hsieh, Baryon masses in lattice QCD with exact chiral symmetry, *Nucl. Phys. A* **755**, 471 (2005).
- [38] C. Alexandrou, J. Carbonell, D. Christaras, V. Drach, M. Gravina, and M. Papinutto, Strange and charm baryon masses with two flavors of dynamical twisted mass fermions, *Phys. Rev. D* **86**, 114501 (2012).
- [39] Y. Namekawa *et al.* (PACS-CS), Charmed baryons at the physical point in 2+1 flavor lattice QCD, *Phys. Rev. D* **87**, 094512 (2013).
- [40] Z. S. Brown, W. Detmold, S. Meinel, and K. Orginos, Charmed bottom baryon spectroscopy from lattice QCD, *Phys. Rev. D* **90**, 094507 (2014).
- [41] K. U. Can, G. Erkol, M. Oka, and T. T. Takahashi, Look

- inside charmed-strange baryons from lattice QCD, *Phys. Rev. D* **92**, 114515 (2015).
- [42] H. Bahtiyar, K. U. Can, G. Erkol, P. Gubler, M. Oka, and T. T. Takahashi, Charmed baryon spectrum from lattice QCD near the physical point, *Phys. Rev. D* **102**, 054513 (2020).
- [43] J.-B. Li, L.-C. Gui, W. Sun, J. Liang, and W. Qin, Triply charmed baryons mass decomposition from lattice QCD (2022), [arXiv:2211.04713](https://arxiv.org/abs/2211.04713) [hep-lat].
- [44] Y. Lyu, H. Tong, T. Sugiura, S. Aoki, T. Doi, T. Hatsuda, J. Meng, and T. Miyamoto, Dibaryon with Highest Charm Number near Unitarity from Lattice QCD, *Phys. Rev. Lett.* **127**, 072003 (2021).
- [45] S. Durr, G. Koutsou, and T. Lippert, Meson and Baryon dispersion relations with Brillouin fermions, *Phys. Rev. D* **86**, 114514 (2012).
- [46] R. A. Briceno, H.-W. Lin, and D. R. Bolton, Charmed-Baryon Spectroscopy from Lattice QCD with $N_f = 2+1+1$ Flavors, *Phys. Rev. D* **86**, 094504 (2012).
- [47] C. Alexandrou, V. Drach, K. Jansen, C. Kallidonis, and G. Koutsou, Baryon spectrum with $N_f = 2+1+1$ twisted mass fermions, *Phys. Rev. D* **90**, 074501 (2014).
- [48] C. Alexandrou and C. Kallidonis, Low-lying baryon masses using $N_f = 2$ twisted mass clover-improved fermions directly at the physical pion mass, *Phys. Rev. D* **96**, 034511 (2017).
- [49] Y.-C. Chen and T.-W. Chiu (TWQCD), Lattice QCD with $N_f = 2 + 1 + 1$ domain-wall quarks, *Phys. Lett. B* **767**, 193 (2017).
- [50] C. Alexandrou, S. Bacchio, G. Christou, and J. Finkenrath, Low-lying baryon masses using twisted mass fermions ensembles at the physical pion mass, *Phys. Rev. D* **108**, 094510 (2023).
- [51] E. Follana, Q. Mason, C. Davies, K. Hornbostel, G. P. Lepage, J. Shigemitsu, H. Trotter, and K. Wong (HPQCD, UKQCD), Highly improved staggered quarks on the lattice, with applications to charm physics, *Phys. Rev. D* **75**, 054502 (2007).
- [52] A. Bazavov *et al.* (MILC), Lattice QCD Ensembles with Four Flavors of Highly Improved Staggered Quarks, *Phys. Rev. D* **87**, 054505 (2013).
- [53] A. Bazavov, C. Bernard, N. Brown, C. DeTar, A. X. El-Khadra, E. Gámiz, S. Gottlieb, U. M. Heller, J. Komijani, A. S. Kronfeld, J. Laiho, P. B. Mackenzie, E. T. Neil, J. N. Simone, R. L. Sugar, D. Toussaint, and R. S. Van de Water (Fermilab Lattice and MILC Collaborations), b - and d -meson leptonic decay constants from four-flavor lattice qcd, *Phys. Rev. D* **98**, 074512 (2018).
- [54] *This supplemental material provides further information pertaining to the lattice QCD ensembles and mass extraction procedures in this study of triply charmed baryons (Ω_{ccc}), along with a compilation of our results on mass splittings and continuum extrapolation. This supplemental material also contains citations to Refs. [84–96].*
- [55] H. Neuberger, Exactly massless quarks on the lattice, *Phys. Lett. B* **417**, 141 (1998).
- [56] H. Neuberger, More about exactly massless quarks on the lattice, *Phys. Lett. B* **427**, 353 (1998).
- [57] N. Mathur, M. Padmanath, and S. Mondal, Precise predictions of charmed-bottom hadrons from lattice QCD, *Phys. Rev. Lett.* **121**, 202002 (2018).
- [58] P. Junnarkar, N. Mathur, and M. Padmanath, Study of doubly heavy tetraquarks in Lattice QCD, *Phys. Rev. D* **99**, 034507 (2019).
- [59] N. Mathur and M. Padmanath, Lattice qcd study of doubly charmed strange baryons, *Phys. Rev. D* **99**, 031501(R) (2019).
- [60] M. Padmanath, A. Radhakrishnan, and N. Mathur, Bound Isoscalar Axial-Vector $bcu\bar{d}\bar{d}$ Tetraquark T_{bc} from Lattice QCD Using Two-Meson and Diquark-Antidiquark Variational Basis, *Phys. Rev. Lett.* **132**, 201902 (2024).
- [61] A. Radhakrishnan, M. Padmanath, and N. Mathur, Study of the isoscalar scalar $bcu\bar{d}\bar{d}$ tetraquark T_{bc} with lattice QCD, *Phys. Rev. D* **110**, 034506 (2024).
- [62] N. Mathur, M. Padmanath, and D. Chakraborty, Strongly Bound Dibaryon with Maximal Beauty Flavor from Lattice QCD, *Phys. Rev. Lett.* **130**, 111901 (2023).
- [63] C. Michael, Adjoint Sources in Lattice Gauge Theory, *Nucl. Phys. B* **259**, 58 (1985).
- [64] M. Luscher and U. Wolff, How to Calculate the Elastic Scattering Matrix in Two-dimensional Quantum Field Theories by Numerical Simulation, *Nucl. Phys. B* **339**, 222 (1990).
- [65] J. Sakurai, *Advanced Quantum Mechanics*, Always learning (Pearson Education, Incorporated, 1967).
- [66] S. Basak, R. Edwards, G. T. Fleming, U. M. Heller, C. Morningstar, D. Richards, I. Sato, and S. J. Wallace (Lattice Hadron Physics (LHPC)), Clebsch-Gordan construction of lattice interpolating fields for excited baryons, *Phys. Rev. D* **72**, 074501 (2005).
- [67] S. Datta, S. Gupta, M. Padmanath, J. Maiti, and N. Mathur, Nucleons near the QCD deconfinement transition, *JHEP* **02**, 145.
- [68] M. Padmanath, *Baryons from lattice QCD*, Ph.D. thesis, TIFR Mumbai (2014).
- [69] I. Montvay and G. Munster, *Quantum fields on a lattice*, Cambridge Monographs on Mathematical Physics (Cambridge University Press, 1997).
- [70] S. Borsanyi *et al.*, High precision scale setting on the lattice, *PoS LATTICE2021*, 371 (2022).
- [71] M. F. L. Golterman, STAGGERED MESONS, *Nucl. Phys. B* **273**, 663 (1986).
- [72] C. Aubin and K. Orginos, A new approach for Delta form factors, *AIP Conf. Proc.* **1374**, 621 (2011).
- [73] Z. Renqiang, S. Wei, C. Feiyu, C. Ying, G. Ming, J. Xiangyu, and L. Zhaofeng, Annihilation diagram contribution to charmonium masses *, *Chin. Phys. C* **46**, 043102 (2022).
- [74] D. Hatton, C. T. H. Davies, B. Galloway, J. Koponen, G. P. Lepage, and A. T. Lytle (HPQCD), Charmonium properties from lattice $QCD+QED$: Hyperfine splitting, J/ψ leptonic width, charm quark mass, and a_μ^c , *Phys. Rev. D* **102**, 054511 (2020).
- [75] O. Bar, C. Bernard, G. Rupak, and N. Shoreh, Chiral perturbation theory for staggered sea quarks and Ginsparg-Wilson valence quarks, *Phys. Rev. D* **72**, 054502 (2005).
- [76] J.-W. Chen, D. O'Connell, and A. Walker-Loud, Universality of mixed action extrapolation formulae, *JHEP* **04**, 090.
- [77] M. Lujan, A. Alexandru, Y. Chen, T. Draper, W. Freeman, M. Gong, F. X. Lee, A. Li, K. F. Liu, and N. Mathur (QCD Collaboration), Δ_{mix} parameter in the overlap on domain-wall mixed action, *Phys. Rev. D* **86**, 014501 (2012).
- [78] S. Basak, S. Datta, N. Mathur, A. T. Lytle, P. Majumdar, and M. Padmanath (ILGTI), Hadron spectra and Δ_{mix} from overlap quarks on a HISQ sea, *PoS LATTICE2014*, 083 (2015).

- [79] B. Mohan, T. Mary S., A. Hazra, and R. Dhir, Screening of the quark charge and mixing effects on transition moments and m_1 decay widths of baryons, *Phys. Rev. D* **106**, 113007 (2022).
- [80] C. McNeile, C. T. H. Davies, E. Follana, K. Hornbostel, and G. P. Lepage, Heavy meson masses and decay constants from relativistic heavy quarks in full lattice QCD, *Phys. Rev. D* **86**, 074503 (2012).
- [81] R. J. Dowdall, C. T. H. Davies, T. C. Hammant, and R. R. Horgan, Precise heavy-light meson masses and hyperfine splittings from lattice QCD including charm quarks in the sea, *Phys. Rev. D* **86**, 094510 (2012).
- [82] B. Chakraborty, C. T. H. Davies, B. Galloway, P. Knecht, J. Koponen, G. C. Donald, R. J. Dowdall, G. P. Lepage, and C. McNeile, High-precision quark masses and QCD coupling from $n_f = 4$ lattice QCD, *Phys. Rev. D* **91**, 054508 (2015).
- [83] S. Basak, S. Datta, M. Padmanath, P. Majumdar, and N. Mathur, Charm and strange hadron spectra from overlap fermions on HISQ gauge configurations, *PoS LATTICE2012*, 141 (2012).
- [84] A. Bazavov *et al.* (MILC), Gradient flow and scale setting on MILC HISQ ensembles, *Phys. Rev. D* **93**, 094510 (2016).
- [85] S. Basak, S. Datta, A. T. Lytle, M. Padmanath, P. Majumdar, and N. Mathur, Hadron spectra from overlap fermions on HISQ gauge configurations, *PoS LATTICE2013*, 243 (2014).
- [86] R. C. Johnson, ANGULAR MOMENTUM ON A LATTICE, *Phys. Lett. B* **114**, 147 (1982).
- [87] A. Bazavov *et al.* (MILC), Scaling studies of QCD with the dynamical HISQ action, *Phys. Rev. D* **82**, 074501 (2010).
- [88] A. Bazavov *et al.*, B - and D -meson leptonic decay constants from four-flavor lattice QCD, *Phys. Rev. D* **98**, 074512 (2018).
- [89] A. Bazavov *et al.* (MILC), Nonperturbative QCD Simulations with 2+1 Flavors of Improved Staggered Quarks, *Rev. Mod. Phys.* **82**, 1349 (2010).
- [90] M. F. L. Golterman and J. Smit, Lattice Baryons With Staggered Fermions, *Nucl. Phys. B* **255**, 328 (1985).
- [91] J. A. Bailey, Staggered baryon operators with flavor SU(3) quantum numbers, *Phys. Rev. D* **75**, 114505 (2007).
- [92] C. DeTar and S.-H. Lee, Variational method with staggered fermions, *Phys. Rev. D* **91**, 034504 (2015).
- [93] J. Balog, F. Niedermayer, and P. Weisz, Logarithmic corrections to $o(a^2)$ lattice artifacts, *Physics Letters B* **676**, 188 (2009).
- [94] N. Husung, Logarithmic corrections to $O(a)$ and $O(a^2)$ effects in lattice QCD with Wilson or Ginsparg–Wilson quarks, *Eur. Phys. J. C* **83**, 142 (2023), [Erratum: *Eur.Phys.J.C* 83, 144 (2023)].
- [95] N. Husung, Lattice artifacts of local fermion bilinears up to $O(a^2)$, (2024).
- [96] S. Navas *et al.* (Particle Data Group Collaboration), Review of particle physics, *Phys. Rev. D* **110**, 030001 (2024).

Supplemental material

This supplemental material provides further information pertaining to the lattice QCD ensembles and mass extraction procedures in this study of triply charmed baryons (Ω_{ccc}), along with a compilation of our results on mass splittings and continuum extrapolation. Towards the end, we also provide a consolidated table of various lattice QCD results in this regard along with various technical details involved.

I. LATTICE DETAILS

We utilize six lattice QCD ensembles with dynamical $N_f = 2 + 1 + 1$ HISQ flavors ($u = d, s, c$; listed in Table II), generated by MILC collaboration [52, 53]. The ensembles $S_1 - S_5$ have a spatial volume of about $(3 \text{ fm})^3$ whereas the ensemble L_1 has a spatial volume of approximately $(4.8 \text{ fm})^3$. The number of measurements (n_{meas}) for the Overlap and HISQ setups are shown in the last two columns respectively. The lattice spacings were measured initially with r_1 parameter [52], which were found to be consistent with scales obtained through Wilson flow [84]. In our previous works using overlap valence action, we also have determined lattice spacings independently using Ω_{sss} mass [57, 85] and found those to be consistent with lattice spacings shown in the column for the study based on overlap valence action. The bare charm quark mass with overlap action was tuned by equating the kinetic mass of the spin average of the 1S charmonia to its physical value following the lattice spacing determination in Refs. [52, 53, 84]. As for the study using HISQ valence quarks, we utilize the valence charm quark mass as listed in Ref. [74], except for the ensemble S_5 , for which we determine it independently by equating the J/ψ mass with its physical value. Naturally we consider the lattice spacings as determined in Ref. [74] for the study with HISQ valence quarks. The resulting uncertainties in mass splitting due to variations in lattice spacings between the different approaches were found to be significantly smaller than the statistical errors, and they remain within a few MeV. We have accounted for these differences in the scale setting uncertainty.

Ensemble	Dimension $N_s^3 \times N_t$	Lattice Spacing (a fm)		n_{meas}	
		Overlap [52, 53, 84]	HISQ [74]	Overlap	HISQ
S_1	$24^3 \times 64$	0.1207(11)	0.12404(67)	294	1400
S_2	$32^3 \times 96$	0.0888(8)	0.09023(48)	188	396
S_3	$48^3 \times 144$	0.0582(4)	0.05926(33)	186	386
S_4	$64^3 \times 192$	0.0441(2)	0.04406(27)	142	400
S_5	$96^3 \times 288$	–	0.03271(20)	–	451
L_1	$40^3 \times 64$	0.1189(10)	0.12225(64)	100	200

TABLE II. Details of the lattice QCD ensembles utilized for calculations with Overlap and HISQ valence quarks.

II. MASS EXTRACTION WITH OVERLAP FERMIONS

We utilize the operator structure proposed in Ref. [66] for the Ω_{ccc}^{++} baryon in building the correlation matrices. Owing to the inherent color antisymmetric and trivially flavor symmetric structure of the Ω_{ccc}^{++} baryon, only symmetric total spin (J) structures are allowed by the total antisymmetric wavefunction for local Ω_{ccc}^{++} baryon operators. This constrains the allowed total spin-parity combination to the symmetric spin state is $J^P = 3/2^+$, which reduces to the H^+ irreducible representation (irrep) of the cubic group on the lattice [86]. With the full four component Dirac spinor, there are two possible embeddings of the H^+ irrep, as listed in Table III in the Dirac-Pauli representation of γ -matrices. This setup ensures that the symmetries of the baryon are faithfully represented in our lattice calculations.

In the Dirac-Pauli representation of the γ matrices [65], the solutions of the Dirac equation suggest the lower two components (3,4) to vanish in the nonrelativistic limit, where the velocity goes to zero. In this sense, the upper two components that survive the nonrelativistic limit are referred to as nonrelativistic, and the lower two as relativistic. Within this γ matrix representation, one of the embedding denoted by ${}^1H^+$ is purely built out of the upper two components and hence is referred to as the nonrelativistic embedding. The second embedding denoted by ${}^2H^+$ carries lower components of the quark spinor reflecting its relativistic nature and hence is referred to as relativistic.

We utilize operators from both these embeddings to form an operator basis and construct 2×2 correlation matrices for baryons. We analyze these correlation matrices variationally following the solution of a generalized eigenvalue

S_z	Op. [N]	Spin	Op. [R]	Spin
+3/2	${}^1H_{+3/2}$	$\{111\}_S$	${}^2H_{+3/2}$	$\{133\}_S$
+1/2	${}^1H_{+1/2}$	$\{112\}_S$	${}^2H_{+1/2}$	$\{233\}_S + \{134\}_S + \{143\}_S$
-1/2	${}^1H_{-1/2}$	$\{122\}_S$	${}^2H_{-1/2}$	$\{144\}_S + \{234\}_S + \{243\}_S$
-3/2	${}^1H_{-3/2}$	$\{222\}_S$	${}^2H_{-3/2}$	$\{244\}_S$

TABLE III. Allowed spin structure of local single flavored baryon operator with the full four component Dirac spinor for quarks. S_z refers to the third component of the baryon spin in the infinite volume continuum. ${}^1H^+$ refers to the nonrelativistic [N] and ${}^2H^+$ to the relativistic [R] embedding, with $\{xyz\}_S = xyz + yzx + zxy$ representing symmetrized spin structure of the baryons, where x, y, z refer to the Dirac spinor components of the quark.

problem (GEVP) and subsequent numerical fits with the expected asymptotic forms for the eigenvalue correlators given by

$$C_{ij}(t)v_{jn} = \lambda_n(t, t_0)C_{ij}(t_0)v_{jn} \text{ and } \lim_{t-t_0 \rightarrow \infty} \lambda_n(t, t_0) = A e^{-m_n(t-t_0)}. \quad (4)$$

The eigenvalue correlators display a few timeslices early saturation of ground state domination when compared to the behavior in a single correlation function and hence aid in a more reliable energy extraction of the ground state mass. t_0 is chosen as a timeslice where the ground state energy plateauing starts as one increases the time interval. We present the effective masses and energy fit estimates for the positive and negative parity Ω_{ccc} baryon ground state in different ensembles in Fig. 5 demonstrating the signal quality.

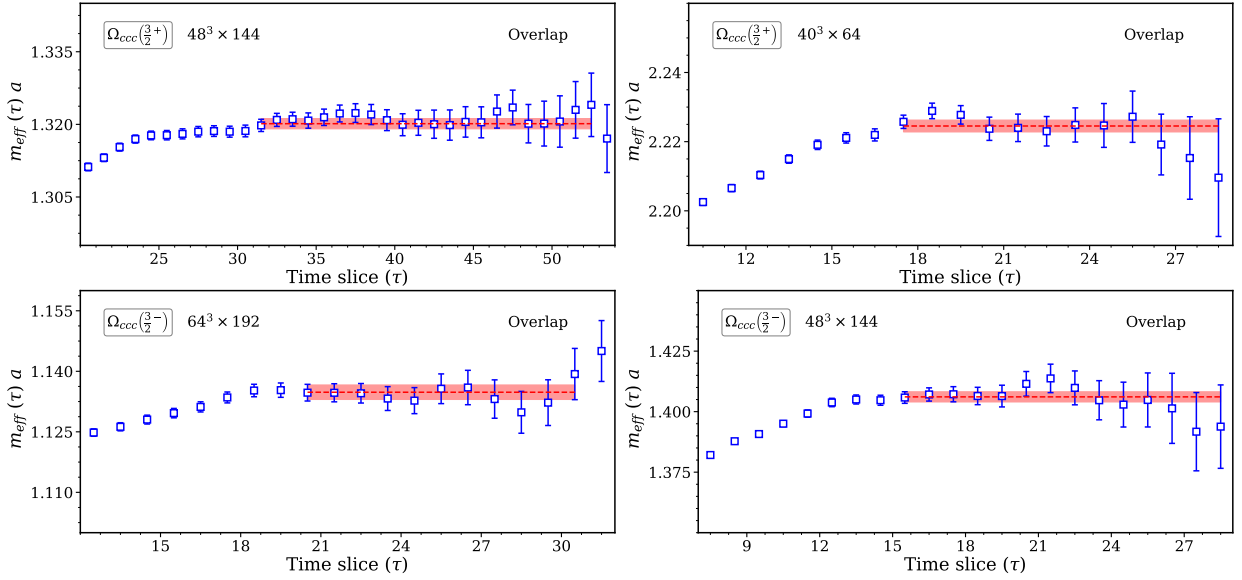


FIG. 5. Effective mass plots corresponding to the positive (top) and negative (bottom) parity lowest energy levels of $\Omega_{ccc}(3/2)$ baryons for different lattice ensembles. The dashed lines are the fit results with one exponential fits, and the bands show the fit ranges with the corresponding 1σ errors.

Baryon correlators are typically noisier compared to that for mesons. One way to improve the signal quality in baryon correlators is by utilizing their antisymmetric nature (for fermions) along the temporal direction. As a result of this feature, baryon correlators will carry signals for positive parity states in the forward direction from the source timeslice, whereas in the backward direction from the source timeslice, signals for negative parity baryon states with the same total spin dominate [67–69]. We take advantage of this property to investigate the lightest spin 3/2 Ω_{ccc} baryons with both parities and also to increase the statistics by investigating forward/backward propagations of correlation matrices in the H^+ and H^- irreps. The interpolators in the H^- irrep can be built from a parity transformation to the H^+ irrep interpolators, which amounts to an interchange of Dirac spinor indices ($1 \leftrightarrow 3$) and ($2 \leftrightarrow 4$) in the Dirac-Pauli representation of γ matrices. The large time behaviour of forward propagating correlators in the H^+ and H^- irreps can be expressed as [68]:

$$\begin{aligned} C_{H^+}(\tau) &\propto c_+ e^{-m_B + \tau} + c_- e^{-m_B - (N\tau - \tau)}, \\ C_{H^+}(\tau) &\propto c_- e^{-m_B - \tau} + c_+ e^{-m_B + (N\tau - \tau)}. \end{aligned} \quad (5)$$

Here, c_+ and c_- are normalization factors in the correlator, while m_{B^+} and m_{B^-} are the masses associated with the positive and negative parity baryon states. In Fig. 6, we present the forward and backward (time inversed to follow a forward propagation for the sake of comparison) propagating correlation functions (left) in the H^+ and H^- irreps and the respective effective masses (right). It can be seen that the forward propagating correlator in the H^+ irrep matches with the backward propagating correlator in the H^- irrep, whereas the forward propagating correlator in the H^- irrep matches with the backward propagating correlator in the H^+ irrep. These two cases represent the positive and negative parity Ω_{ccc} spin 3/2 baryon respectively. This consistency is transparent in the effective masses presented in the figure. As one would naively expect, it can also be seen that the negative parity state has a relatively heavier effective mass, which can also be inferred from the steeper slope in the correlation function plotted on the left.

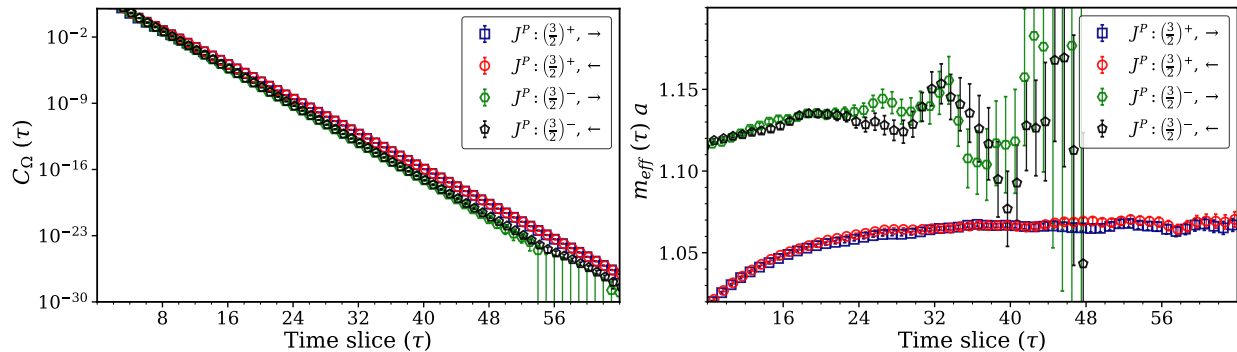


FIG. 6. Correlators and corresponding effective masses for Ω_{ccc} baryons on the $48^3 \times 144$ lattice ensembles. In the legend, (\rightarrow) indicates forward propagation, while (\leftarrow) represents backward propagation (time inversed to follow a forward propagation for the sake of comparison).

III. MASS EXTRACTION WITH HISQ FERMIONS

We utilize six $N_f = 2 + 1 + 1$ dynamical MILC lattice ensembles [52, 87, 88] details of which are provided in Table II. We use fat7 smeared gauge links with Lepage term in the fermion action [51, 89]. We also utilize the three-link (Naik) term in the HISQ fermion action for the valence quarks. The correction to the Naik term is tuned using dispersion relations of η_c and J/ψ mesons. The values of the lattice spacing for these ensembles are taken from Ref. [74]. As in Ref. [74], on each of these ensembles, we tune the charm quark mass by equating lattice extracted J/ψ meson mass with its experimental value.

To extract the ground state masses of η_c and J/ψ mesons, we use local 0-link spin-taste naive quark bilinears [51, 71]. The relevant operators utilized in this work are the following,

$$\mathcal{O}^\eta = \bar{c}\gamma_5 \otimes \xi_5 c, \quad \mathcal{O}_i^{J/\psi} = \bar{c}\gamma_i \otimes \xi_i c, \quad (6)$$

where the γ and ξ matrices act on spinor and taste degrees of freedom of the c quark field, respectively. For Ω_{ccc} baryons, we utilize the following operator [90],

$$\mathcal{O}_{\Omega_{ccc}}(t) = \epsilon_{abc} D_1 c^a(\mathbf{x}, t) D_2 c^b(\mathbf{x}, t) D_3 c^c(\mathbf{x}, t). \quad (7)$$

Here, $c^a(\mathbf{x}, t)$ is the staggered charm quark field and a, b and c are the color indices and the action of D_i operators on $c^a(\mathbf{x}, t)$ amount to, $D_i c^a(\mathbf{x}, t) = \frac{1}{2} (c^a(\mathbf{x} - \hat{i}, t) + c^a(\mathbf{x} + \hat{i}, t))$. The flavor wavefunction of $\mathcal{O}_{\Omega_{ccc}}$ is fully symmetric, while the color wavefunction is totally antisymmetric. This operator transforms in the $8'$ irreps of geometric time slice (GTS) group and lies in the A_2^- irreps of the octahedral group (\mathcal{O}_h). Details about this operator can be found in Refs. [90, 91]. With HISQ quarks this operator couples to Ω baryons with two different tastes, and they are degenerate only in the continuum limit. At a finite lattice spacing, this leads to a difference in Ω_{ccc} baryons masses with a splitting of $\mathcal{O}(\alpha_s(1/a)(m_c a)^2)$. This systematic can be accounted for by incorporating this term in the continuum extrapolation.

A. Extracting the Ground State Masses

We extract the masses of 1S charmonia (η_c , J/ψ) and Ω_{ccc} baryons by studying the exponential decays of their respective two point correlation functions,

$$C_O^{2-pt}(t) = \sum_{\mathbf{x}} \langle 0 | \mathcal{O}(\mathbf{x}, t) \overline{\mathcal{O}}(\mathbf{x}_{src}, t_{src}) | 0 \rangle, \quad (8)$$

at large source-sink separation. Here, \mathcal{O} represent their respective interpolating operators as discussed above. As in the overlap case, we use a wall-source point-sink setup. The standard procedure of staggered quarks with relevant phase factors is followed.

By introducing a complete set of states in between two interpolating operators at the source and sink, one can show that the above two point correlation function simplifies to,

$$C_O^{2-pt}(t) = \sum_{i=0}^{\infty} |\mathcal{Z}_i|^2 (e^{-E_i \tau} + e^{-E_i(n_t - \tau)}) - \sum_{i=0}^{\infty} (-)^{\tau} |\mathcal{Z}_i^o|^2 (e^{-E_i^o \tau} + e^{-E_i^o(n_t - \tau)}). \quad (9)$$

Here, i runs over all possible finite volume eigenstates with increasing energy that can couple to their respective interpolating fields. The superscript “o” in E_i^o of the second term represents the oscillating contributions from the opposite parity states. The time-oscillating terms in the above equation appear as the staggered interpolating operators also couple to their respective opposite parity states with a phase oscillation in time [51, 71]. At a large source-sink separation ($\tau = t - t_{src}$), the ground state ($i = 0$) dominates the correlation function with a functional form,

$$C_O^{2-pt}(t) \approx |\mathcal{Z}_0|^2 (e^{-E_0 \tau} + e^{-E_0(n_t - \tau)}) - (-)^{\tau} |\mathcal{Z}_0^o|^2 (e^{-E_0^o \tau} + e^{-E_0^o(n_t - \tau)}), \quad \text{for } t \gg t_{src}. \quad (10)$$

As in Ref. [92], to determine the ground state mass of a single hadron, we employ the following strategy. To mitigate the oscillating phase, we first smooth out the two-point correlation function with appropriate time-shiftings, leading to the following asymptotic form,

$$\overline{C^{2-pt}}(t)^2 \approx |\mathcal{Z}_0|^4 e^{-2E_0 \tau} (1 + (-)^{\tau} \mathcal{R} (1 - \cosh \Delta) e^{-\Delta \tau} + \mathcal{O}(e^{-2\Delta \tau})), \quad t \gg t_{src}. \quad (11)$$

Here, $\overline{C^{2-pt}}(t)$ is the smoothed correlation function, $\Delta = E_0^o - E_0$, and $\mathcal{R} = \frac{|\mathcal{Z}_0^o|^2}{|\mathcal{Z}_0|^2}$. Since $\Delta > 0$ and large, the oscillating term in Eq. (11) gets highly suppressed beyond $t \geq 15$. For our fittings, we typically use $\tau \geq 15$ for the ensembles S1 and S2, while those are ≥ 25 for the ensembles S3, S4, and S5.

Next, we construct a correlation matrix using these time-shifted smoothed correlation functions [72],

$$\mathbb{C}(t) = \begin{pmatrix} \overline{C^{2-pt}}(t) & \overline{C^{2-pt}}(t+1) \\ \overline{C^{2-pt}}(t+1) & \overline{C^{2-pt}}(t+2) \end{pmatrix}. \quad (12)$$

With such a correlation matrix, we then follow the standard GEVP procedure [63, 64] to extract the lowest energy levels for the positive and negative parity Ω_{ccc} baryons.

In Fig. 7, we show the representative effective mass plots on two different ensembles for the lowest energy levels of $\Omega_{ccc}(3/2^+)$ (top pane) and $\Omega_{ccc}(3/2^-)$ (bottom pane) baryons. The fit ranges and 1σ fit errors are shown by the colored band. Following the methods mentioned above, we extract the ground state masses for η_c , J/ψ , $\Omega_{ccc}(3/2^+)$, and $\Omega_{ccc}(3/2^-)$. We use both one and two exponential fits and observe no difference in fit values of the lowest state (much below percent level) at large τ . After extracting the individual masses we calculate the 1S charmonia hyperfine splitting, $M_{J/\psi} - M_{\eta_c}$, and $\Omega_{ccc} - \frac{3}{2}M_{c\bar{c}}$, with $c\bar{c} \equiv J/\psi$ and $\overline{1S}$ charmonia. The whole procedure is performed using the bootstrap method.

IV. RESULTS ON MASS SPLITTINGS AND CONTINUUM EXTRAPOLATION

In Table IV we show these mass splittings for each lattice ensemble. The errorbars in each fit include 1σ fit errors. Results using two different valence quark actions are presented in the separate columns for Overlap and HISQ.

A. Hyperfine splitting in 1S charmonia

The 1S charmonia splittings extracted on different ensembles at finite lattice spacings are presented in the second column of Table IV. Following this, we proceed with the continuum extrapolation of these splittings. Since both

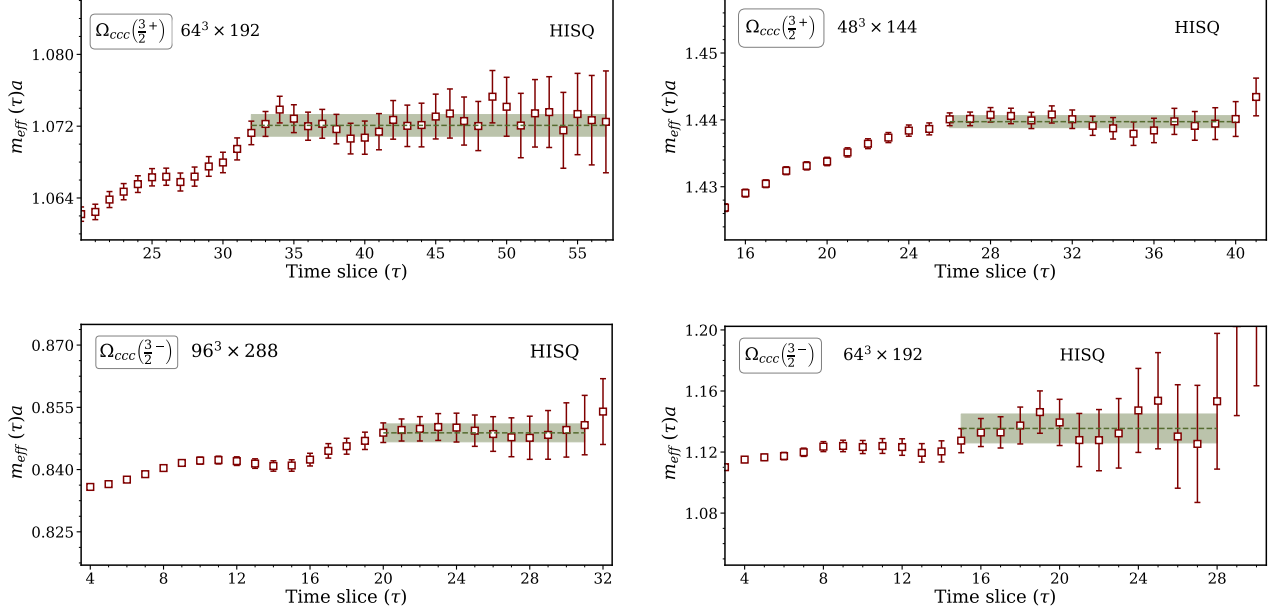


FIG. 7. Effective mass plots corresponding to the positive (top) and negative (bottom) parity lowest energy levels of $\Omega_{ccc}(3/2)$ baryons for different lattice ensembles. The dashed lines are the fit results with one exponential fits, and the bands show the fit ranges with the corresponding 1σ errors.

Lattice Ensembles	$M_{J/\psi} - M_{\eta_c}$		$M_{\Omega_{ccc}(\frac{3}{2})^+} - \frac{3}{2}M_{J/\psi}$		$M_{\Omega_{ccc}(\frac{3}{2})^+} - \frac{3}{2}M_{\overline{1S}}$		$M_{\Omega_{ccc}(\frac{3}{2})^-} - \frac{3}{2}M_{J/\psi}$		$M_{\Omega_{ccc}(\frac{3}{2})^-} - \frac{3}{2}M_{\overline{1S}}$	
	Overlap	HISQ	Overlap	HISQ	Overlap	HISQ	Overlap	HISQ	Overlap	HISQ
S_5		116.09 ± 1.15		149.77 ± 3.61		192.41 ± 3.72		458.17 ± 15.11		500.81 ± 15.21
S_4	113.0 \pm 2.0	113.25 ± 1.16	147.14 ± 3.79	150.86 ± 5.61	189.29 ± 3.67	193.22 ± 5.64	448.89 ± 8.25	431.72 ± 23.15	491.04 ± 8.20	474.10 ± 23.07
S_3	119.0 \pm 2.0	110.71 ± 0.83	147.68 ± 3.86	149.50 ± 3.20	192.11 ± 3.78	191.01 ± 3.24	439.15 ± 7.03	430.14 ± 11.89	483.59 ± 6.98	471.65 ± 11.96
S_2	126.5 \pm 2.0	105.79 ± 1.14	147.88 ± 5.69	148.85 ± 3.61	195.47 ± 5.61	188.52 ± 3.65	438.35 ± 14.03	427.96 ± 15.62	485.94 ± 14.00	467.62 ± 15.66
S_1	147.0 \pm 1.5	106.44 ± 0.33	135.80 ± 5.70	159.12 ± 1.97	190.64 ± 5.63	199.04 ± 1.98	392.06 ± 10.80	467.54 ± 17.88	446.89 ± 10.76	507.45 ± 17.89
L_1	146.0 \pm 1.5	106.94 ± 0.42	129.91 ± 3.03	158.50 ± 2.09	184.49 ± 2.96	198.61 ± 2.11	401.42 ± 13.05	442.32 ± 37.34	455.99 ± 13.04	482.42 ± 37.35

TABLE IV. Extracted mass differences (in units of MeV) obtained by fitting the individual correlators and then taking the difference of fitted masses by bootstrapping. The subtracted masses are obtained using both $c\bar{c} \equiv J/\psi$ and $\overline{1S}$ in Eq. (2) of the main paper. We also show here the hyperfine splitting in 1S-charmonia. Results for both HISQ and overlap quarks are shown.

the overlap and HISQ actions are free from $\mathcal{O}(ma)$ errors, the leading term in the extrapolation is expected to be of $\mathcal{O}((ma)^2)$. We use three different fit ansatz; (i) $f_1(a) = c_1 + c_2a^2$, (ii) $f_2(a) = c_1 + c_2a^2 + c_3a^4$, and (iii) $f_3(a) = c_1 + c_2a^2 + c_4a^2 \log a$. The last form is motivated from the expectation that for an asymptotically free theory the leading asymptotic lattice spacing dependence may have $a^2 \log(a^{n=1})$ term, rather than a simple integer power-law term [93–95]. The fit results are presented in Table V and shown in Fig 8 with colored bands representing the 1σ fit errors. The stars at the continuum limit are the extrapolated values while solid red square represents the physical value of the hyperfine splitting. Notably, the approach to the continuum limit differs between the two versions of the discretized lattice actions: the overlap results approach from above, while the HISQ results approach from below. The results obtained with overlap quarks are below the physical value but remain consistent with it, whereas the results with HISQ quarks are just above the physical value. HISQ results also agree with that obtained in Ref. [74]. As noted in Ref. [74], this discrepancy could be attributed to the exclusion of the charm self-annihilation diagrams while

calculating η_c mass. This contribution to J/ψ correlation function appears at order $\mathcal{O}(\alpha_s^3)$ based on power counting of strong coupling α_s whereas this contributes to η_c correlation function at order $\mathcal{O}(\alpha_s^2)$. A lattice calculation also found the η_c mass increases by 3 – 4 MeV, whereas the effects on J/ψ mass are negligible at the level of per-mille precision [73]. This effect survives at the continuum limit and hence results in a discrepancy between lattice and physical results. For the overlap valence quarks, because of two different actions in sea and valence sectors, an extra systematic appears which is proportional to Δ_{mix} in the mixed action formalism [75–77]. This term needs to be accounted in the continuum extrapolation and can amount to a systematic of a few MeV [78].

Fitting Model	Splitting(MeV)		$\chi^2/\text{d.o.f.}$	
	Overlap	HISQ	Overlap	HISQ
$f_1(a) = c_1 + c_2 a^2$	110.0 ± 2.2	116.3 ± 0.9	1.14	1.35
$f_2(a) = c_1 + c_2 a^2 + c_3 a^4$	110.9 ± 3.2	117.7 ± 1.2	0.79	1.21
$f_3(a) = c_1 + c_2 a^2 + c_4 a^2 \log a$	112.5 ± 5.2	120.9 ± 1.8	0.92	0.73

TABLE V. Continuum extrapolation results for the hyperfine splitting ($M_{J/\psi} - M_{\eta_c}$). The first column lists the fitting ansatz, the second column provides the continuum extrapolated values in MeV, and the third column reports the respective $\chi^2/\text{d.o.f.}$

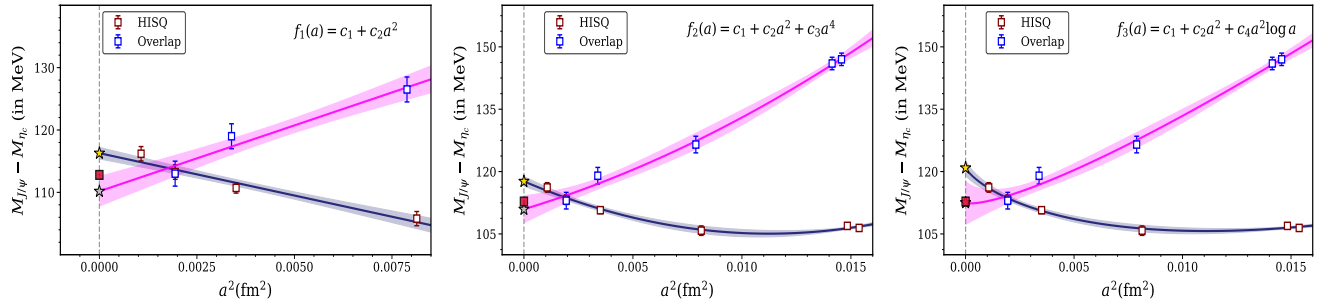


FIG. 8. Continuum extrapolation of the hyperfine splitting ($M_{J/\psi} - M_{\eta_c}$) for both overlap and HISQ valence quarks. Left: Extrapolation using fitting model $f_1(a)$ from Table V; Middle: with fitting model $f_2(a)$; Right: with fitting model $f_3(a)$. Considering the possibility of higher order discretization, we do not include the coarsest ensembles S_1 and L_1 with the fit form $f_1(a)$. The 1σ bands are estimated using the bootstrap resampling method, while the magenta square on the $a^2 = 0$ line represents the PDG average of $(M_{J/\psi} - M_{\eta_c}) = 112.8 \pm 0.4$ MeV [96].

B. Continuum extrapolation and estimation of Ω_{ccc} masses

In Table IV, we present the subtracted masses (as in Eq. (2) of the main draft) both for the overlap and HISQ quarks. Results are obtained at various lattice spacings within a range $\sim 0.12 - 0.032$ fm. Next, we perform the continuum extrapolation of these mass splittings. As in the case of the continuum limit of hyperfine splitting, we use the following fit ansatzes: (i) $f_1(a) = c_1 + c_2 a^2$ and (ii) $f_2(a) = c_1 + c_2 a^2 + c_3 a^4$. Along with that, for HISQ quark we also include a fitting form similar to Eq. (5) of Ref. [74] (iiia) $f_3(a) = c_1 + c_2 a^2 + c_5 \alpha_s (1/a) (m_c a)^2$, and $f_4(a) = c_1 + c_4 a^4 + c_5 \alpha_s (1/a) (m_c a)^2$, where α_s is the strong-coupling constant and $m_c a$ is the bare charm quark mass. The fitted results are presented in Tables VI and VII.

Fitting Model	$M_{\Omega_{ccc}}(3/2^+) - \frac{3}{2}M_{J/\psi}$ (MeV)		$\chi^2/\text{d.o.f.}$	
	Overlap	HISQ	Overlap	HISQ
$f_1(a) = c_1 + c_2 a^2$	147.1 ± 4.3	149.7 ± 3.2	0.1	0.16
$f_2(a) = c_1 + c_2 a^2 + c_3 a^4$	144.3 ± 6.2	151.3 ± 4.3	1.08	0.12
$f_3(a) = c_1 + c_2 a^2 + c_5 \alpha_s (1/a) (m_c a)^2$	–	148.5 ± 7.9	–	0.15
$f_4(a) = c_1 + c_4 a^4 + c_5 \alpha_s (1/a) (m_c a)^2$	–	150.6 ± 3.7	–	0.1

TABLE VI. Continuum extrapolation results for the subtracted mass $[M_{\Omega_{ccc}}(3/2^+) - \frac{3}{2}M_{J/\psi}]$, using various possible fit ansatzes. Results are shown both for overlap and HISQ valence quarks.

Fitting Model	$M_{\Omega_{ccc}}(3/2^+) - \frac{3}{2}M_{\overline{1S}} \text{ (MeV)}$		$\chi^2/\text{d.o.f.}$	
	Overlap	HISQ	Overlap	HISQ
$f_1(a) = c_1 + c_2a^2$	187.9 ± 4.2	193.0 ± 3.2	0.1	0.26
$f_2(a) = c_1 + c_2a^2 + c_3a^4$	185.2 ± 6.4	194.8 ± 4.3	1.03	0.31
$f_4(a) = c_1 + c_4a^4 + c_5\alpha_s(1/a)(m_c a)^2$	—	194.3 ± 3.8	—	0.78

TABLE VII. Similar to Table VI, but for energy splittings $[M_{\Omega_{ccc}}(3/2^+) - \frac{3}{2}M_{\overline{1S}}]$.

In Fig. 9 and 10, we depict the above fitted results, for $[M_{\Omega_{ccc}}(3/2^+) - \frac{3}{2}M_{J/\psi}]$ and $[M_{\Omega_{ccc}}(3/2^+) - \frac{3}{2}M_{\overline{1S}}]$, respectively. In the left panes, on these figures, we show the results with the quadratic fit forms $f_1(a)$. Note we do not use the coarser lattices, S_1 and L_1 ensembles, in this case to avoid higher order discretization at largest lattice spacing. The extrapolated results at the continuum limit are shown by the star symbols. The solid square is a symmetrized average of two results obtained with the fit form $f_1(a)$, with the errorbar covering both the Overlap and HISQ fit errors. In the right panes, we show results by including both quadratic and quartic terms in lattice spacings, $f_2(a)$. The thin line includes 1σ errors covering both the fit ansatzs, $f_1(a)$ and $f_2(a)$.

Note that, unlike in the charmonia, there is no charm annihilation contribution in the lattice mass estimation of Ω_{ccc} baryons. Since J/ψ meson mass has a much lesser contribution from such effect, we choose our final values from the subtracted mass, $M_{\Omega_{ccc}} - M_{J/\psi}$. Given that our estimate for Ω_{ccc} baryon is arrived at following independent approaches to continuum of the energy splittings from the spin average of the $1S$ charmonia as well as the J/ψ meson mass, these effects due to charm annihilation are well under 1 MeV errors. Consistency between the Ω_{ccc} baryon mass estimates from either of these approaches gives further confidence in our numbers.

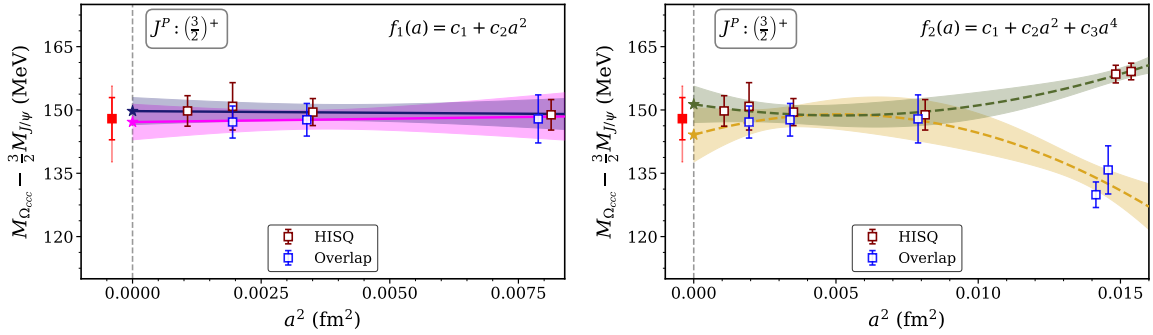


FIG. 9. Continuum extrapolation of the subtracted mass splitting, $M_{\Omega_{ccc}}(3/2^+) - \frac{3}{2}M_{J/\psi}$, for both the Overlap and HISQ actions. Left: Extrapolation using the quadratic fitting ansatz, $f_1(a)$, as in Table VI. Here the coarser lattices, S_1 and L_1 ensembles, are not included since they may have higher order discretization. Right: same with the ansatz of quadratic and quartic terms in lattice spacings, $f_2(a)$, fitted with all data points. The extrapolated results at the continuum limits are shown by the star symbols. The 1σ confidence bands are estimated using the bootstrap resampling method. The solid square is a symmetrized average of two results obtained with the fit form $f_1(a)$, with the errorbar covering both the Overlap and HISQ fit errors. The thin line includes 1σ errors from the fit ansatzs $f_1(a)$ and $f_2(a)$.

The corresponding continuum extrapolated results for the negative parity state, $[M_{\Omega_{ccc}}(3/2^-) - \frac{3}{2}M_{c\bar{c}}]$, with $c\bar{c} \equiv J/\psi$ and $\overline{1S}$ charmonia, are tabulated in Tables VIII and IX respectively. Here again, different possible fit forms are employed to find the extent of discretization effects. The fit results are also presented in Figs. 11 and 12, respectively, with the similar symbols and color-coding as in Figs. 9 and 10.

Fitting Model	$M_{\Omega_{ccc}}(3/2^-) - \frac{3}{2}M_{J/\psi} \text{ (MeV)}$		$\chi^2/\text{d.o.f.}$	
	Overlap	HISQ	Overlap	HISQ
$f_1(a) = c_1 + c_2a^2$	448.6 ± 10.8	449.0 ± 12.8	0.52	0.72
$f_2(a) = c_1 + c_2a^2 + c_3a^4$	441.6 ± 16.8	458.1 ± 17.4	0.56	0.38

TABLE VIII. Continuum extrapolation results for the splitting $[M_{\Omega_{ccc}}(3/2^-) - \frac{3}{2}M_{J/\psi}]$ with various fit ansatzs for the Overlap and HISQ actions.

Next we present the mass splitting between $\Omega_{ccc}(3/2)^-$ and $\Omega_{ccc}(3/2)^+$ baryons, in Table X. For this mass splitting we do not use the ratio method as the fit ranges for the ground states of $\Omega_{ccc}(3/2)^-$ and $\Omega_{ccc}(3/2)^+$ are different.

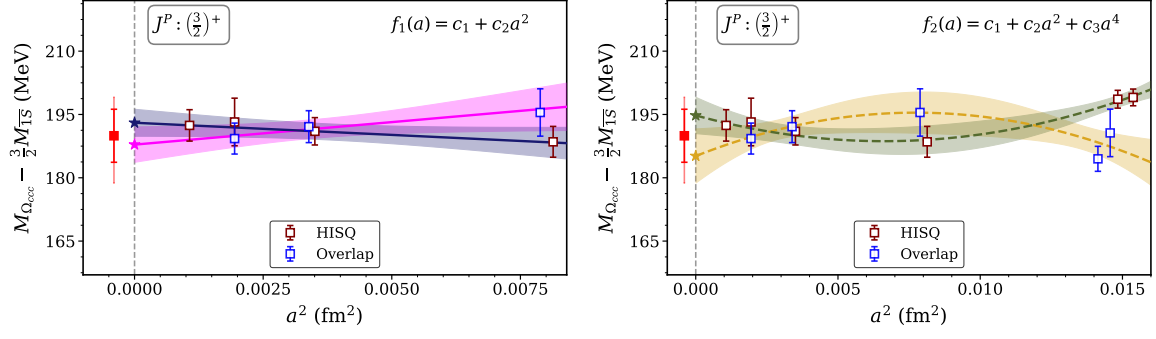


FIG. 10. Continuum extrapolation of the subtracted mass splitting, $M_{\Omega_{ccc}}(3/2^+) - \frac{3}{2}M_{\overline{15}}$, for both the Overlap and HISQ actions. All other details are as in Fig. 9.

Fitting Model	$M_{\Omega_{ccc}}(3/2^-) - \frac{3}{2}M_{\overline{15}}$ (MeV)		$\chi^2/\text{d.o.f.}$	
	Overlap	HISQ	Overlap	HISQ
$f_1(a) = c_1 + c_2 a^2$	489.5 ± 10.7	492.7 ± 13.9	0.39	0.76
$f_2(a) = c_1 + c_2 a^2 + c_3 a^4$	480.7 ± 16.7	501.5 ± 18.9	0.47	0.39

TABLE IX. Continuum extrapolation results for the energy splitting $[M_{\Omega_{ccc}}(3/2^-) - \frac{3}{2}M_{\overline{15}}]$ with various fit ansatzs for the Overlap and HISQ actions.

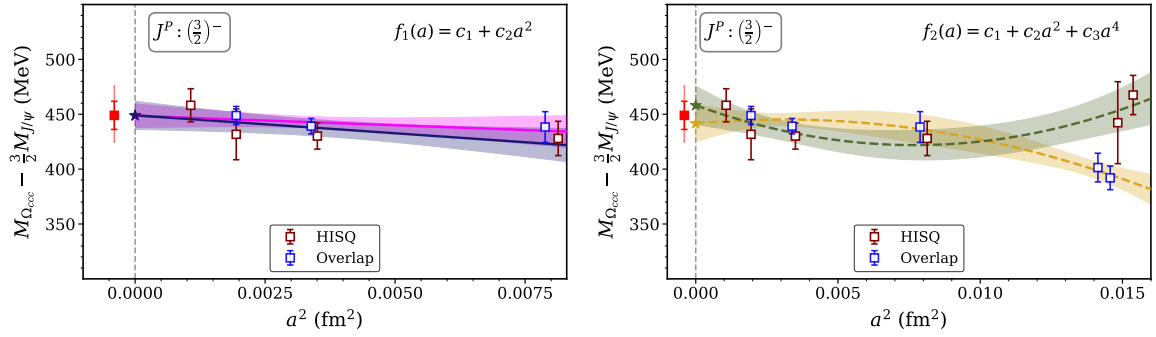


FIG. 11. Continuum extrapolation of the subtracted mass splitting, $[M_{\Omega_{ccc}}(3/2^-) - \frac{3}{2}M_{J/\psi}]$, for both the Overlap and HISQ actions. The fit results are presented in Table VIII. All other details are as in Fig. 9.

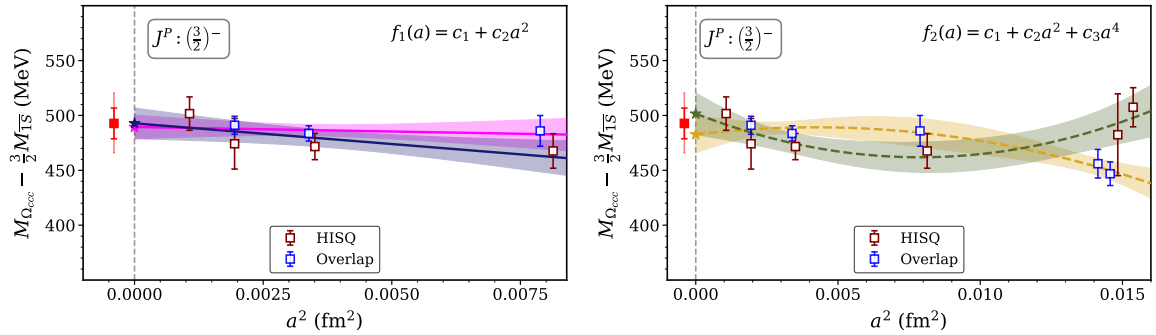


FIG. 12. Continuum extrapolation of the subtracted mass splitting, $[M_{\Omega_{ccc}}(3/2^-) - \frac{3}{2}M_{\overline{15}}]$, for both the Overlap and HISQ actions. The fit results are presented in Table IX. All other details are as in Fig. 9.

Instead, we use the difference in their fit values within the bootstrap procedure. In Fig. 13 we show these fit results. The continuum extrapolated results are shown by the star symbol, and the solid red square is our final value with the thick bar as the 1σ error. The thin bar at the continuum point shows the extent of discretization considering the

fit forms, f_1 and f_2 . Our final result for this mass splitting is: $\Omega_{ccc}(3/2)^-$ and $\Omega_{ccc}(3/2)^+ = 301(13)(14)$ MeV, with statistical and systematic errors respectively.

Lattice Ensembles	$M_{\Omega_{ccc}(\frac{3}{2})^-} - M_{\Omega_{ccc}(\frac{3}{2})^+}$ (MeV)	
	Overlap	HISQ
S_5		308.41 ± 15.78
S_4	301.76 ± 8.84	280.86 ± 23.59
S_3	291.47 ± 7.82	280.64 ± 12.77
S_2	290.47 ± 15.00	279.11 ± 16.24
S_1	256.26 ± 12.06	308.42 ± 18.23
L_1	271.51 ± 13.33	283.82 ± 37.81

TABLE X. The mass splitting between the lowest energy levels of positive and negative parity Ω_{ccc} baryons.

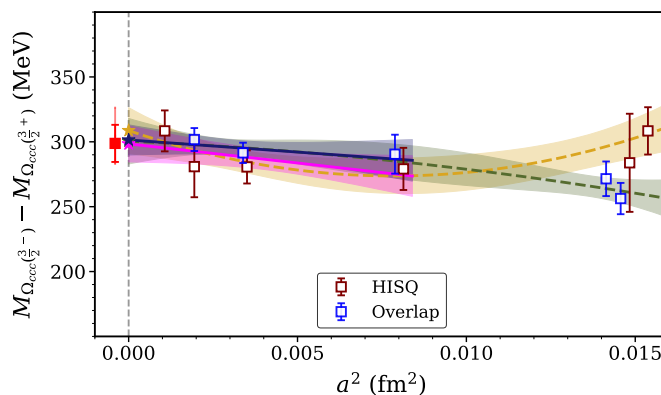


FIG. 13. Continuum extrapolation of the energy splitting between the ground state masses of $\Omega_{ccc}(\frac{3}{2}^-)$ and $\Omega_{ccc}(\frac{3}{2}^+)$ baryons. Color scheme: magenta and blue solid line represents the fit results using the fit form i) $\Delta M(a) = c_1 + c_2 a^2$, for the HISQ and overlap valence actions, respectively. The green and yellow dashed line show the fit results using the fit form ii) $\Delta M(a) = c_1 + c_2 a^2 + c_3 a^4$, for the HISQ and overlap valence action, respectively. The stars indicate the continuum extrapolated values, whereas the red square is a symmetrized average of results from either procedures, with thick errorbars representing the errors from quadratic extrapolation. The thin errorbar account the uncertainties arising out of difference in results between quadratic and quartic extrapolations.

In Table XI we tabulate the results obtained by various lattice QCD collaborations for the ground states of $\Omega_{ccc}(3/2^+)$ and $\Omega_{ccc}(3/2^-)$ baryons. The references are shown in the first column. Note that, in addition to other details, we have also highlighted whether continuum extrapolations were included in these calculations. Results from this work are listed in the last row.

V. ELECTROMAGNETIC CORRECTION

The presence of two units of electric charge is expected to affect the mass of the Ω_{ccc}^{++} baryons. A naive perturbative estimate for the leading order electromagnetic correction to the mass should be proportional to $\alpha_{em} \hbar c / r_c$, where α_{em} is the electromagnetic fine structure coefficient, whereas $\hbar c / r_c$ is the natural energy scale corresponding to r_c , the root-mean-square charge radius of the Ω_{ccc}^{++} baryon. Using $\alpha_{em} = 1/137$ and the lattice-determined estimate for $r_c = 0.410(6)$ fm from Ref. [41], one can find that this correction is approximately 3.5 MeV.

To elaborate this assessment, one could apply the standard time independent perturbation theory, by assuming the Coulombic interaction potential as a perturbative part and a trial wave function for the Ω_{ccc}^{++} baryon ground state that could provide an upper bound for this electromagnetic correction. To this end, we consider two trial wave

Ref. (Year)	N_f	$a(fm)$	m_π (MeV)	S_q^{sea}	S_c^{val}	Continuum Extrapolation	$M_{\Omega_{ccc}(\frac{3}{2}^+)}$ (MeV)	$M_{\Omega_{ccc}(\frac{3}{2}^-)}$ (MeV)
[37] (2005)	quench	0.0882	-	Wilson	DW	No	4681(28)	5066(48)
[38] (2012)	2,2+1	0.056-0.089	260-470	TM	OS	Yes (3)	4677(5)(3)	-
[46] (2012)	2+1+1	0.06-0.12	220-310	HISQ	RHQA	Yes (3)	4761(52)(21)(6)	-
[83] (2012)	2+1+1	0.06-0.09	316-329	HISQ	Overlap	No	4765(10)	-
[45] (2012)	2	0.0728	280	Clover	Brillouin	No	4774(24)	-
[39] (2013)	2+1	0.0899	135	Clover	RHQA	No	4789(22)	-
[2] (2013)	2+1	0.0351	390	Clover	Clover	No	4763(7)	5124(14)
[47] (2014)	2+1+1	0.065-0.094	210-430	TM	OS	Yes (3)	4734(12)(11)(9)	-
[40] (2014)	2+1	0.085-0.11	227-419	DW	RHQA	Yes (2)	4796(8)(18)	-
[41] (2015)	2+1	0.0907	156	Wilson	Clover	No	4769(6)	-
[48] (2017)	2	0.0938	130	TM Clover	OS	No	4746(4)(32)	-
[49] (2017)	2+1+1	0.063	280	DW	DW	No	4766(5)(11)	5168(37)(51)
[42] (2020)	2+1	0.0907	156	Clover	Clover	No	4817(12)	5083(67)
[44] (2021)	2+1	0.0846	146	Clover	RHQA	No	4796(1)	-
[43] (2022)	2+1	0.0711-0.0828	278-300	DW	Overlap	No	4793(21)	5071(27)
[50] (2023)	2+1+1	0.057-0.080	137-141	TM Clover	OS	Yes (3)	4785(71)	-
This work	2+1+1	0.0327-0.1207	216-329 [53]	HISQ	HISQ, Overlap	Yes (5)	4793(5)(7)	5094(12)(13)

TABLE XI. A compilation of all lattice results for masses of $\Omega_{ccc}(3/2^+)$ and $\Omega_{ccc}(3/2^-)$, along with various relevant technical details involved. The result from this work is presented in the bottom most row. Several relevant lattice specific details listed above include: the number of dynamical quark flavors (N_f), lattice spacing (a), pion mass (m_π), as well as the actions employed for the sea ($S^{sea}q$) and valence charm quarks ($S^{val}c$) in each work. Additionally, it is indicated whether the calculation includes a continuum extrapolation, and if so, the number of distinct lattice spacings used in the extrapolation is indicated inside brackets. Abbreviations: HISQ (highly-improved staggered quark action), DW (Domain-wall), TW (Twisted mass), OS (Osterwalder-Seiler), and RHQA (relativistic heavy-quark action). Quoted values are rounded to the nearest integer. For calculations on multiple lattice spacings without continuum extrapolation, results from the finest lattice are listed.

functions that respects the symmetries of the Ω_{ccc}^{++} baryon ground state and has the same root-mean-square charge radius $r_c = \sqrt{\langle \psi | r^2 | \psi \rangle}$. The first choice is the 1S radial solution of Hydrogen atom which has been utilized also in Ref. [44], and the second one is a Gaussian wavefunction in the radial direction, as given below,

$$\psi_1(\mathbf{r}) = \left(\frac{8}{\pi a^3}\right)^{1/2} \exp\left(-\frac{2|\mathbf{r}|}{a}\right), \quad (13)$$

$$\psi_2(\mathbf{r}) = \left(\frac{2}{\pi a^2}\right)^{3/4} \exp\left(-\frac{|\mathbf{r}|^2}{a^2}\right). \quad (14)$$

The parameter a is chosen to be as $a = 2r_c/\sqrt{3}$, such that the average charge radius is r_c for both choices of wavefunctions. With these two ansatzs, the leading order corrections are given by, $\frac{5}{2\sqrt{3}} \alpha_{em} \hbar c / r_c$ and $\frac{4}{\sqrt{3}\pi} \alpha_{em} \hbar c / r_c$, respectively. It is evident from the expressions that the leading order electromagnetic corrections are of the same order ($\alpha_{em} \hbar c / r_c$) and is independent of the trial wave function, modulo factors $\mathcal{O}(1)$. This amounts to the corrections 5.1 MeV and 4.6 MeV, respectively, which are in good agreement with the previous estimate.